

Original Research

cGAS/STING/NLRP3 Signaling Pathway-Mediated Pyroptosis in Hypertrophic Cardiomyopathy Radiotherapy

Huiyang Li¹, Xin Wang², Xinping Luo¹, Haiming Shi¹, Jian Li^{1,*}

Academic Editors: Natascia Tiso and Kavindra Kumar Kesari

Submitted: 10 August 2024 Revised: 29 November 2024 Accepted: 17 December 2024 Published: 5 March 2025

Abstract

Background: Radiotherapy is a commonly employed treatment modality for cancer; however, its radiobiological effects in hypertrophic cardiomyopathy (HCM) remain unclear. Radiation exposure activates the cyclic guanosine monophosphate-adenosine monophosphate (cGAMP) synthase (cGAS)-stimulator of interferon genes (STING) pathway, which is functionally associated with the activation of NOD-like Receptor (NLR) family pyrin domain containing 3 (NLRP3) inflammasomes, known mediators of pyroptotic cell death. Nonetheless, the underlying mechanism requires further investigation. Therefore, the objective of this study is to elucidate the role of the cGAS/STING/NLRP3 pathway in the process of cardiomyocyte pyroptosis during radiotherapy for HCM. Methods: Transverse aortic constriction surgery was conducted to establish a mouse model of pressure overload-induced HCM, followed by the administration of 30 Gray (Gy) radiation one-week post-surgery. Cardiac morphology and function were evaluated through echocardiographic techniques. Hematoxylin & Eosin staining, along with Wheat Germ Agglutinin (WGA) staining, were utilized to quantify the cross-sectional area of cardiomyocytes and the degree of left ventricular hypertrophy. The HL-1 mouse cardiac muscle cell line was subjected to 40 Gy of radiation using an X-ray irradiator to establish an in vitro model of HCM, with or without the application of the NLRP3 inhibitor MCC950 and cGAS overexpression. Various assays, including the Cell Counting Kit-8 (CCK8), enzyme-linked immunosorbent assay (ELISA), and 5,5',6,6'-tetrachloro-1,1',3,3'-tetraethylbenzimi- dazolylcarbocyanine iodide (JC-1) probe assays, were performed to assess cell viability, the concentrations of Interleukin (IL)- 1β , IL-18, and cGAMP, as well as mitochondrial membrane potential. The morphology of cell membranes and mitochondria was analyzed using scanning electron microscopy (SEM) and fluorescence in situ hybridization (FISH) dual labelling techniques. The expression levels of cGAS, STING, and NLRP3 were evaluated through by western blot analysis. Results: Radiotherapy reduced cardiac hypertrophy, improved cardiac function, and decreased fibrotic changes in HCM mice when compared to control groups. The application of radiation resulted in pyroptosis in HL-1 cells and a reduction in cell viability; this effect that was alleviated by the inhibition of NLRP3, while overexpression of cGAS exacerbated the situation. Furthermore, radiation led to a decline in mitochondrial membrane potential and the leakage of mitochondrial DNA into the cytoplasm, which activated the cGAS-STING signaling pathway, thereby initiating pyroptosis. This activation was corroborated by elevated levels of pyroptosis-associated proteins, including eGAS, STING, NLRP3, caspase-1, Gasdermin D (GSDMD), eGAMP, IL-18, and IL-1β. Notably, the inhibition of NLRP3 effectively abolished the upregulation of IL-18, and IL-1 β levels. Conclusion: Radiation can improve cardiac function, decrease hypertrophy of myocardial cells, and induce oxidative stress. This oxidative stress results in the leakage of mitochondrial DNA (mtDNA), which subsequently activates the cGAS/STING/NLRP3 signalling pathway, culminating in pyroptosis.

Keywords: hypertrophic cardiomyopathy; radiotherapy; cGAS; STING; NLRP3; pyroptosis

1. Introduction

Hypertrophic cardiomyopathy (HCM) is characterized by left ventricular hypertrophy and is estimated to affect approximately 0.2% of the general population [1–3]. Contemporary therapeutic strategies have significantly transformed HCM into a condition that is highly manageable, resulting in low mortality rates. The standard management of HCM typically involves pharmacological agents such as calcium channel blockers and beta-blockers to mitigate disease progression. In certain cases, invasive interventions, including septal myectomy, percutaneous septal ablation, and the implantation of cardioverter-defibrillators (ICDs), may be warranted [4]. Especially, non-invasive

treatment modalities, such as stereotactic body radiotherapy (SBRT), exhibit promising potential for the management of HCM. SBRT is a highly precise radiation therapy that delivers high doses in fewer sessions, targeting tumors while minimizing collateral damage to adjacent healthy tissues, often employing advanced imaging and positioning technologies. Its therapeutic efficacy is attributed to both direct cytotoxic effects on tumor cells and indirect mechanisms, including vascular damage and immune system activation [2,5,6]. SBRT has emerged as a promising non-invasive treatment modality for various non-malignant conditions, including arrhythmias [7], coronary artery in-stent restenosis [8], trigeminal neuralgia [9], refractory epilepsy [10],

¹Department of Cardiology, Huashan Hospital, Fudan University, 200040 Shanghai, China

²CyberKnife Center, Huashan Hospital, Fudan University, 200040 Shanghai, China

^{*}Correspondence: 13816066763@163.com (Jian Li)

and tremors [11], due to its precise targeting and favourable safety profiles. In the context of cardiac disorders, existing literature suggests that SBRT is a safe non-invasive intervention for ventricular tachycardia, as evidenced by the short-term evaluations following treatment [12–14]. A study by Li et al. [15] highlighted the successful application of SBRT in five patients with drug-refractory symptomatic HCM, utilizing 4D-computed tomography (CT) imaging to monitor respiratory and cardiac motion during the procedure. The administration of a radiation dose of 25 Gray (Gy) resulted in an improved prognosis for the patient, with no significant adverse effects reported during follow-up, indicating that SBRT may be a viable non-invasive option for patients with drug-refractory symptomatic HCM. Furthermore, research conducted by Li et al. [2] on both basic and clinical levels demonstrated that a radiation dose of 40 Gy significantly reduced the spontaneous beating frequency and regional thickness of neonatal rat cardiomyocytes. In a rabbit model of HCM, the administration of 20-40 Gy resulted in a reduction in septal thickness and a decrease in the left ventricular weight-to-body weight ratio. In a clinical setting, three patients with HCM exhibited improved clinical symptoms following SBRT, with no severe adverse reactions noted during a four-week follow-up period. Collectively, these findings underscore the feasibility, efficacy, and safety of SBRT as a treatment for HCM [2]. Nonetheless, there are ongoing, challenges in refining treatment protocols, comprehending the long-term consequences, and elucidating the underlying mechanisms associated with various conditions [16]. To date, limited research has addressed the radiobiological effects of SBRT in patients with cardiac patients, given that radiation exposure can induce DNA double-strand breaks and mitochondrial dysfunction, which may ultimately result in cellular apoptosis and tissue injury [17]. To improve the clinical utilization of SBRT, a more comprehensive of its mechanisms is necessary.

The processes by which radiation induces cellular damage predominantly involve the impairment of DNA due to high-energy ionizing radiation (IR) and the detrimental effects of reactive oxygen species (ROS) on cellular components. IR can result in various forms of DNA damage, including strand chain breaks, cross-linking, and structural alterations, which ultimately lead to cell cycle arrest and cell death [18]. Furthermore, IR promotes the generation of ROS, such as hydroxyl radicals and hydrogen peroxide, which inflict damage on essential macromolecules, including proteins, lipids, and nucleic acids, thereby contributing to cellular injury. As a result, the mechanisms associated with radiosensitization primarily concentrate on promoting apoptosis, modifying cell cycle distribution, enhancing the indirect cellular effects of ROS generated by radiotherapy, and impairing the cellular capacity to repair DNA damage [19]. The cyclic guanosine monophosphate-adenosine monophosphate (cGAMP) syn-

thase (cGAS)-stimulator of interferon genes (STING) signaling pathway represents an intracellular immune response mechanism that is activated by cytosolic DNA and mediates immune response [20]. Radiation-induced oxidative stress can lead to the release of mitochondrial DNA (mtDNA) into the cytoplasm, which subsequently activates the cGAS-STING signaling cascade [21]. During tumor radiotherapy, the irradiation of tumor cells results in the accumulation of DNA or RNA fragments within the cytoplasm, thereby triggering the cGAS-STING signalling pathway that detects these nucleic acids. In addition, the cGAS-STING signaling cascade plays a crucial role in regulating the expression of type I interferons (IFN- α/β) expression, thereby enhancing the immune response against tumors [22]. In the context of tumor immunotherapy, the cGAS-STING pathway has emerged as a significant target for inducing pyroptosis, particularly in the context of overcoming resistance to radio-immunotherapy [23]. Empirical studies indicate that the cGAS-STING pathway is capable of triggering programmed cell death mechanisms, which may include apoptotic processes mediated by absent in melanoma 2 (AIM2) or NLR family pyrin domain containing 3 (NLRP3) inflammasomes [24,25]. The production of mitochondrial ROS can lead to oxidative damage to mtDNA, which is subsequently released into the cytoplasm, thereby activating cGAS-STING-mediated pyroptosis [26,27]. Pyroptosis is initiated by the activation of caspase-1 or caspase-11 through the NLRP3 inflammasome. While pyroptosis shares morphological characteristics with both apoptosis and necrosis, it can be differentiated from these other forms of programmed cell death by its distinctive features, which include cell swelling, membrane rupture, DNA damage, and the release of pro-inflammatory cytokines [28]. Furthermore, NLRP3 inflammasome-mediated pyroptosis has been associated with a variety of pathological conditions, including cardiovascular diseases [29]. However, the specific role of NLRP3 inflammasome-mediated pyroptosis in the radiobiological effects of radiotherapy for HCM remains inadequately elucidated.

To date, there have been no studies specifically investigating the cGAS/STING/NLRP3 signaling pathway in the context of radiotherapy for HCM. Nevertheless, the established role of this pathway in various cardiovascular diseases, coupled with the recognized impact of radiation on oxidative stress and mitochondrial dysfunction, underscores the necessity of investigating its involvement in HCM. Therefore, the aim of this study was to elucidate the mechanisms underlying cGAS/STING/NLRP3 signaling in the context of radiation-induced cardiomyocyte pyroptosis of cardiomyocytes as a therapeutic approach for HCM. In this study, a model of HCM was established in mice through transverse aortic constriction (TAC) surgery, followed by the administration of 30 Gy of radiation one-week post-surgery. Cardiac structure and function were evaluated using echocardiogra-



phy, while histological analyses were conducted to assess cell size. *In vitro* experiments involved exposing HL-1 cells to 40 Gy of X-rays, with or without the NLRP3 inhibitor MCC950 and cGAS overexpression, to replicate HCM conditions. Various assays, including Cell Counting Kit-8 (CCK-8), enzyme-linked immunosorbent assay (ELISA), 5,5',6,6'-tetrachloro-1,1',3,3'-tetraethylbenzimidazolylcarbocyanine iodide (JC-1), and mitochondrial health. Additionally, the protein expressions of cGAS, STING, and NLRP3 were analyzed using western blotting techniques.

2. Materials and Methods

2.1 Animals

C57BL/6J mice aged 6-8 weeks were obtained from the HYcell Biotechnology (Wuhan, China) and allocated into three distinct groups: a sham group (which underwent surgery without ligation), an HCM group, and an HCM group subjected to 30 Gy radiation treatment group (n = 5per group). To create a mouse model of pressure overloadinduced HCM, TAC surgery was performed in accordance with established protocols [30]. In brief, the mice were anesthetized with a combination of 2% isoflurane (AErrane, Baxter, Deerfiel, IL, USA) and 1.0 L/min of 100% oxygen within an induction chamber. A longitudinal skin incision measuring 1.0 cm was made at the suprasternal notch to expose the thymus and aorta. Following this, a 2 mm longitudinal incision was made in the sternum. A bent 26 G needle and a 6-0 silk suture were then employed to ligate the aorta between the right innominate and left common carotid arteries. In the sham control group, identical procedures were executed, with the sole exception that the artery was not subjected to ligation.

One week following the successful establishment of the HCM mouse model, a radiation dose of 30 Gy was administered over a two-week period. The body weights of the mice across all three experimental groups were recorded initially at baseline and subsequently at regular intervals throughout the duration of the study. Observations were conducted regarding mental health status, dietary and water intake, urination and defecation patterns, as well as the condition of the skin in the irradiated area for each group. Any alterations or abnormalities were meticulously documented and monitored. All mice were euthanized via cervical dislocation, and cardiac tissues were subsequently harvested. The mice were provided with humane care and were fed in accordance with the standards set forth in the National Institutes of Health (NIH) Guide for the Care and Use of Laboratory Animals. All animal maintenance and experimental procedures were conducted in compliance with the approval of the Ethics Committee of the Huashan Hospital Institutional Review Board (No 2020 Huashan Hospital JS-590).

2.2 Echocardiography

To assess cardiac morphology and function, echocardiographic analysis was conducted utilizing an ultrasound device (Mylab X5 Vet, Esaote, Genova, Italy), as outlined in a prior study [31]. In summary, mice were subjected to imaging under light anesthesia with a combination of isoflurane (1–2%, AErrane, Baxter, Deerfiel, IL, USA) and oxygen (1 L/min). Systolic and diastolic functions were evaluated through conventional M-mode and two-dimensional echocardiography, augmented by pulse-wave Doppler techniques. A range of parameters was documented, including fractional shortening (FS), left ventricular (LV) ejection fraction (LVEF), systolic posterior wall (SPW) thickness, LV posterior wall (LVPW) thickness, LV internal diastolic (LVID) diameter, LV internal systolic (LVIS) diameter, interventricular septal systolic (IVSS) thickness, interventricular septal diastolic (IVSD) thickness, LV end-diastolic volume, LV end-systolic volume, relative wall thickness, and heart rate. LV volumes were determined by directly tracing of the LV wall contour in the long-axis view to compute volumes at end-diastole and end-systole. For each parameter, three measurements were taken per subject.

2.3 Hematoxylin & Eosin (H&E) and Wheat Germ Agglutinin (WGA) Staining

H&E (Hematoxylin, H9627-25G, Sigma-Aldrich, St Louis, MO, USA; Eosin Y, D12621, Xiya Reagent, Linshu, Shangdong, China) and WGA (L4895-2M, Sigma-Aldrich, St Louis, MO, USA.) staining was performed to evaluate the cross-sectional area of cardiomyocytes and the degree of LV hypertrophy, respectively. Cardiac tissues from the murine subjects were harvested and subsequently fixed in formalin. Following standard protocols for dehydration utilizing ethanol and achieving transparency with xylene, the samples were embedded in paraffin for sectioning. Subsequently, 5 µm sections were then stained with H&E and WGA. Imaging was conducted using an Olympus fluorescence microscope (CX-21, Tokyo, Japan), and the cross-sectional area of the cardiomyocytes was quantified employing the ImageJ software 1.53 (National Institutes of Health, Bethesda, MD, USA).

2.4 Cell Culture

The HL-1 mouse cardiac muscle cell line (SCC065, acquired from Sigma-Aldrich, St.Louis, MO, USA) was cultured in Dulbecco's Modified Eagle Medium (DMEM, 10% FBS, 100 U/mL penicillin, and 100 μg/mL streptomycin). DMEM and penicillin/streptomycin were obtained from Hyclone (SH30023, SH30022, SH30021, SH30265.01B, SH30809, SV30010, Logan, UT, USA), and FBS was purchased from Tianhang (141215, Huzhou, Zhejiang, China). All cell lines underwent validation through short tandem repeat (STR) profiling. All cell lines underwent validation using a MycoProbe Mycoplasma Detection kit (CULoo1B, R&D systems, Minneapolis, MN, USA)



and were confirmed to be free of mycoplasma contamination. The cells were maintained in an incubator under a 5% CO₂ atmosphere at 37 °C until they reached the logarithmic growth phase. At this stage, the HL-1 cells were allocated into several experimental groups: a control group, a radiation group, a NLRP3 inhibitor group, a NLRP3 inhibitor (MCC950, S8930, Selleck, Houston, TX, USA) combined with radiation group, a cGAS overexpression group, and a cGAS overexpression combined with MCC950 and radiation group. The dose-response relationship regarding cell viability post-irradiation was assessed, revealing a decline in cell viability with increasing radiation doses. At a dose of 40 Gy, cell viability approximated the half-maximal inhibitory concentration (IC50), while at 50 Gy, viability fell below the IC50 threshold (refer to Supplementary Fig. 1). Consequently, a radiation dose of 40 Gy was selected for subsequent in vitro experiments with cells in the radiation group receiving a single exposure of 40 Gy via an X-ray irradiator (RS-2000, Radsource, Suwanee, GA, USA.).

2.5 Cell Treatment and Transfection

For the transfection procedure, HL-1 cells were seeded at a density of 1.0×10^5 cells per well in 6-well plates and incubated overnight to allow for adherence. The transfection of the pCDNA3.1-FLAG-cGAS plasmid, which was synthesized by ELK Biotechnology (Wuhan, Hubei, China, refer to **Supplementary Fig. 2**), was performed utilizing Lipofectamine 3000 transfection reagent (11668019, Invitrogen, Carlsbad, CA, USA) in accordance with the manufacturer's guidelines. Control groups were transfected with blank pCDNA3.1 vector. Additionally, to inhibit NLRP3, HL-1 cells were treated with 20 μ M of MCC950.

2.6 CCK-8 Assay

To evaluate cell viability, a CCK-8 assay (C0038, Beyotime, Shanghai, China) was conducted in accordance with the manufacturer's guidelines. A total of 5000 HL-1 cells were plated in each well of a 96-well plate, subjected to various experimental treatments, and incubated overnight. Subsequently, the cells were treated with 10 μL of CCK-8 per well and incubated for a duration of 1–4 hours at 37 °C in an incubator. The optical density at 450 nm (OD450) was then measured using a microplate reader (DR-200BS, Hiwell-Diatek, Wuxi, Jiangsu, China).

2.7 Western Blot

Whole heart tissue samples from the mice or HL-1 cells were subjected to lysis using a cell lysis buffer (AS1004, Aspenbio, Wuhan, Hubei, China) supplemented with a protease inhibitor cocktail (04693159001, Roche Diagnostics, Mannheim, Germany) and phenylmethylsulfonyl fluoride (PMSF, AS1006, Aspenbio, Wuhan, Hubei, China). The protein concentrations were quantified utilizing the BCA method (AS1006, Aspenbio, Wuhan, Hubei,

China). For each well, 10 µg of protein was applied for separation via SDS-PAGE. Following this, the proteins were transferred to polyvinylidene difluoride (PVDF) membranes (Millipore, Bedford, MA, USA) employing a blot transfer apparatus (AS1015, Aspenbio, Wuhan, Hubei, China). After blocking with a blocking solution, the membranes were incubated overnight with primary antibodies, including anti-cGAS (1:1000, 26416-1-AP, Proteintech, Wuhan, Hubei, China), anti-cAMP (1:2000, ab134901, Abcam, Cambridge, UK), anti-STING (1:1000, 19851-1-AP, Proteintech, Wuhan, Hubei, China), anti-NLRP3 (1:1000, 15101, CST, Boston, MA, USA), anti-caspase-1 (1:500, AF5418, Affbiotech, Cincinnati, OH, USA), anticleaved caspase-1 (1:500, 89332, CST, Boston, MA, USA), anti-GSDMD (1:1000, ab219800, Abcam, Cambridge, UK), anti-GSDMD-N (1:1000, 10137, CST, Boston, MA, USA), and anti-β-Actin (1:5000, TDY051, Tdybio, Beijing, China). The following day, after washing the membranes five times, they were incubated with the appropriate secondary antibodies for 30 minutes at room temperature (RT). The secondary antibodies utilized in this study included goat anti-rabbit IgG-HRP, goat anti-mouse IgG-HRP, goat anti-rat IgG-HRP, rabbit anti-goat IgG-HRP, and rabbit anti-sheep IgG-HRP (1:10,000 dilution, BA1055, BA1075, BA1060, Boster, Wuhan, Hubei, China; ab97057, ab6747, Abcam, Cambridge, UK). Detection was performed using ECL substrate (AS1059, Aspenbio, Wuhan, Hubei, China) in accordance with the manufacturer's instructions.

2.8 ELISA

To assess the concentrations of Interleukin (IL)- 1β , IL-18, and cGAMP in the supernatants, we employed Mouse IL-1 and Mouse IL-18 ELISA kits (ELK1271, ELK2269, ELK Biotechnology, Wuhan, Hubei, China), as well as a cGAMP ELISA kit (501700, Cayman, Ann Arbor, MI, USA), following the protocols provided by the manufacturers.

2.9 Mitochondrial Membrane Potential and Morphology

To evaluate the reduction in mitochondrial membrane potential, the JC-1 probe (C2006, Beyotime, Shanghai, China) was employed in accordance with the manufacturer's guidelines. Cells were treated with the JC-1 solution at 37 °C for 30 minutes, ensuring protection from light exposure. Subsequent to the incubation period, the cells were rinsed three times with phosphate-buffered saline (PBS), and the cell nuclei were stained with DAPI (D8417-1MG, Sigma-Aldrich, St Louis, MO, USA) at RT for 20–30 minutes. Following the application of an anti-fade mounting medium, fluorescence microscopy (CX-21, Olympus, Tokyo, Japan) was employed to capture the resulting images.



2.10 Scanning Electron Microscopy

The morphology of cell membranes was analyzed utilizing scanning electron microscopy (SEM) in accordance with established protocols [32]. Briefly, HL-1 cells were cultured on 10 mm glass coverslips and subsequently fixed for 2 h at RT in PBS buffer containing 2% paraformaldehyde and 3% glutaraldehyde. Following fixation, the cells were rinsed with PBS buffer and post-fixed in 1% osmium tetroxide (OsO₄) for 30 minutes. The cells were then dehydrated through a graded series of ethanol solutions. Following ethanol dehydration, the cells underwent critical point drying, were mounted onto stubs, and coated with a thin layer of conductive metal, specifically gold and palladium, via a sputter coating technique. SEM images were captured using the FEI Quanta 650 FEG SEM system (JEOL, Tokyo, Japan), and representative images were selected for inclusion in the results section.

2.11 Fluorescence in Situ Hybridization (FISH) Dual Labelling

To evaluate mitochondrial morphology, HL-1 cells were subjected to dual-labeling with MitoTracker® Red (C1035, Beyotime, Shanghai, China) and PicoGreenTM double-stranded DNA stain (P2023, UElandy, Hangzhou, Zhejiang, China). Briefly, HL-1 cells were incubated with PicoGreenTM stain at RT in the dark for 3 minutes. Following this, the cells were washed three times with PBS and subsequently stained with MitoTracker® Red (100 nM) for 20 minutes at 37 °C, while avoiding exposure to light. The cells were then fixed using 4% paraformaldehyde and counterstained with the nuclear dye DAPI. Imaging was captured by a confocal microscope (TCS SP5, Leica Microsystems, Wetzla, Germany), and the resulting images were analyzed using ImageJ software (version 1.6.0, National Institutes of Health (NIH), Bethesda, MD, USA).to quantify signal intensity.

2.12 Statistical Analysis

Data were analyzed and profiled by GraphPad Prism 9.0 (La Jolla, CA, USA). Prior to statistical analysis, the normality of data distribution was assessed using a combination of the Shapiro-Wilk test and visual inspection methods, such as Q-Q plots and histograms. The results are presented as mean values for each experimental repetition, with the variability within each repetition represented by the standard deviation (\pm SD). For datasets with a normal distribution, comparisons between two groups were conducted using a two-tailed Student's t-test, while comparisons among multiple groups were assessed using a oneway analysis of variance (ANOVA) followed by Tukey's post hoc post-test. For datasets that did not follow a normal distribution or when normality could not be reasonably assumed, non-parametric tests such as the Mann-Whitney U test or Kruskal-Wallis test with Dunn's post hoc test were applied as appropriate. A *p*-value of less than 0.05 was considered statistically significant.

3. Results

3.1 Radiation Attenuates Cardiac Hypertrophy and Improves Cardiac Functions in HCM Mouse Model

Echocardiographic assessments were conducted to evaluate alterations in cardiac morphology and function across three groups of experimental mice, which demonstrated notable differences in several cardiac parameters among the groups (Fig. 1A–C).

In comparison to the sham-operated mice, the mice subjected to pressure overload-induced HCM mice exhibited a significant reduction in LVEF and FS (p < 0.001, Fig. 1D,E), which signifies compromised cardiac function. Additionally, the HCM mouse model displayed an increase in LVPW thickness and SPW thickness (p < 0.001, Fig. 1F,G), indicating the presence of hypertrophic alterations in the myocardium. Furthermore, the HCM mice showed an increase in LVID diameter and LVIS diameter (p < 0.01, Fig. 1H,I), alongside a decrease in IVSD thickness (p < 0.01) and IVSS thickness (p < 0.05, Supplementary Fig. 3A,B), which collectively suggest an expansion of cardiac chamber dimensions.

Notably, the HCM mice that received a radiation dose of 30 Gy exhibited marked enhancements in cardiac function, as indicated by significantly elevated values of EF, FS, LVPW diameter, and systolic posterior wall thickness when compared to the HCM mouse model (Fig. 1D–G). While the LVID and LVIS diameter measurements in the HCM + 30 Gy group remained higher than those observed in the shamoperated mice, they were nonetheless reduced in comparison to the HCM mice (Fig. 1H,I).

The LV end-diastolic and end-systolic volumes were significantly reduced in the HCM + 30 Gy group in comparison to the HCM group (Fig. 1J,K), indicating a potential enhancement in cardiac remodeling. However, there was no observed alteration in the relative wall thickness, which represents the ratio of wall thickness to chamber diameter, between the HCM + 30 Gy radiation group and the HCM group (Fig. 1L). Additionally, no notable changes in heart rate were detected across all three experimental groups (Supplementary Fig. 3C).

The results of this study confirm the effective creation of a mouse model of HCM induced by pressure overload through the use of TAC surgery. Furthermore, the findings indicate that radiotherapy exerts a positive influence on both cardiac morphology and function in the context of HCM.

3.2 Radiation Alleviates Cardiac Hypertrophy and Cardiomyocyte Enlargement

Pathological myocardial hypertrophy often leads to the enlargement of cardiomyocytes, which serves as a significant marker for HCM. Therefore, we performed WGA



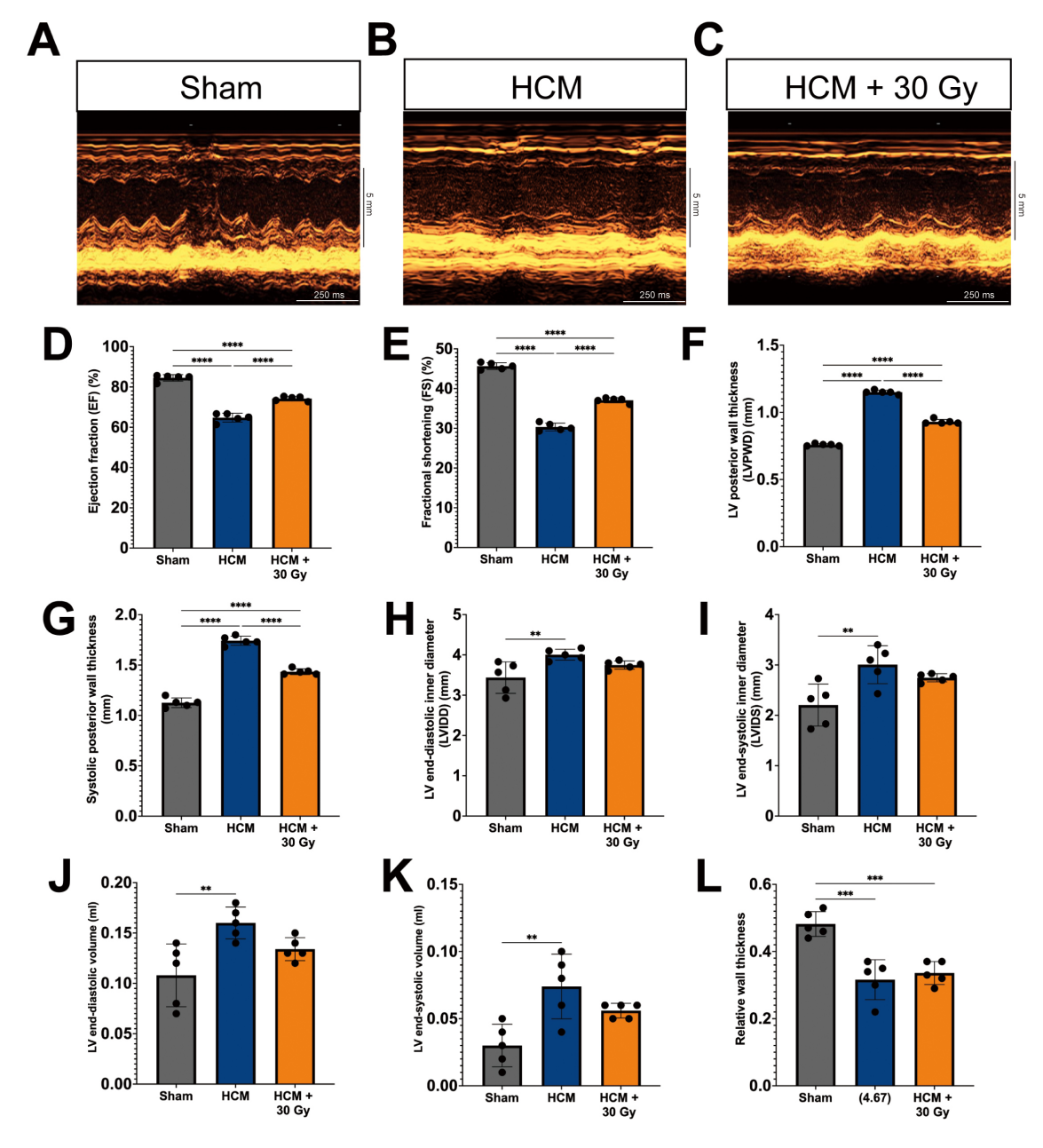


Fig. 1. Radiation attenuates cardiac hypertrophy and improves cardiac function in a pressure overload-induced hypertrophic cardiomyopathy (HCM) mouse model. (A–C) M-mode echocardiography photos for mouse hearts from sham-operated (A), HCM (B), and HCM + radiation mouse groups (C). Scale bars represent 5 mm (vertical axis) and 250 ms (horizontal axis). Quantitative analysis of left ventricular ejection fraction (LVEF) (D), fractional shortening (FS) (E), LV posterior wall (LVPW) thickness (F), systolic posterior wall (SPW) thickness (G), LV internal diastolic (LVID) diameter (H), LV internal systolic (LVIS) diameter (I), LV end-diastolic volume (J), LV end-systolic volume (K), and relative wall thickness (L). Mean \pm SD, n = 5 per group. **p < 0.01, ***p < 0.001, and ****p < 0.0001.

staining to assess the cross-sectional area of cardiomyocytes, as this measurement is a dependable indicator of cellular hypertrophy and other pathological alterations [33,34]. The findings from H&E and WGA staining of paraffinembedded heart tissue sections from three experimental mouse groups demonstrated significant variations in both the cross-sectional area of cardiomyocytes. In sham-operated mice, the cross-sectional area of cardiomyocytes was observed to be within normal limits (mean = 217 μ m²), with no significant hypertrophy detected (Fig. 2A,B,G). Conversely, mice with HCM exhibited a marked increase in cardiomyocyte size (mean = 356 μ m²) when compared to the sham-operated group (p < 0.001, Fig. 2G), which is indicative of cardiac hypertrophy (Fig. 2C,D). Notably, the mean cardiomyocyte size in the



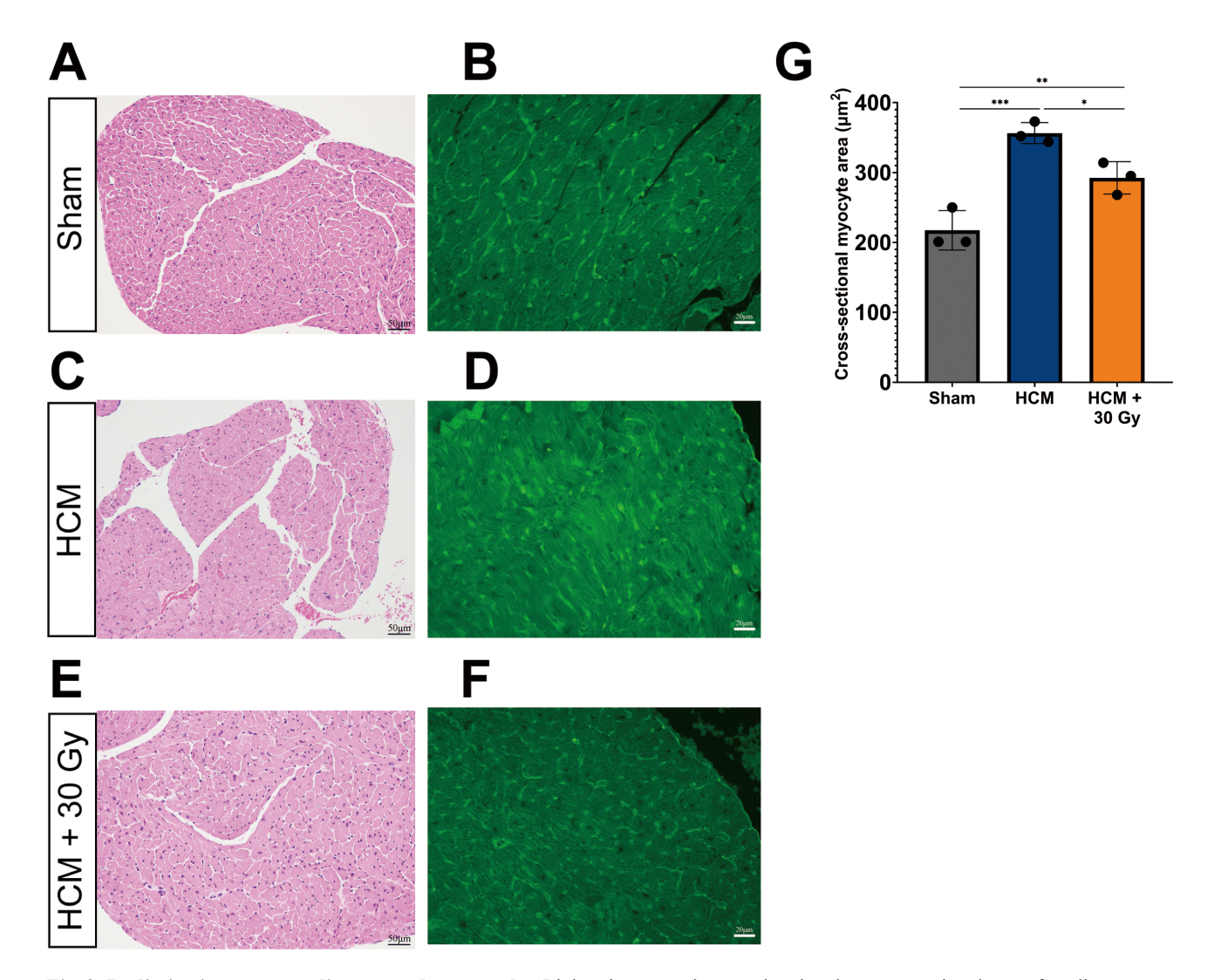


Fig. 2. Radiation improves cardiomyocyte hypertrophy. Light microscope images showing the cross-sectional area of cardiomyocytes of the LV in three experimental mouse groups. Heart tissue sections were immuno-stained with hematoxylin & eosin (H&E) and Wheat Germ Agglutinin (WGA) (green) in sham-operated mice (A,B), HCM mice (C,D), and HCM + radiation mice (E,F). WGA-stained (green) images show myocardial hypertrophy. (A,C,E) the scale bar = 50 μ m. (B,D,F) the scale bar = 20 μ m. (G) Quantification of cross-sectional myocyte area in sham-operated, HCM, and HCM + radiation mice. *p < 0.05, **p < 0.01, and ***p < 0.001.

HCM + 30 Gy group (mean = 292 μ m²) remained significantly larger than that of the sham group (p < 0.01); however, radiation treatment resulted in a significant reduction in cardiomyocyte size relative to the HCM group (p < 0.05, Fig. 2G), suggesting a potential attenuation of cardiac hypertrophy (Fig. 2E,F). Furthermore, the degree of LV hypertrophy appeared to be diminished in HCM mice subjected to radiation compared to their untreated counterparts (Fig. 2F vs. Fig. 2D), indicating a possible beneficial effect of radiation therapy on myocardial pathological changes. These results imply that radiation treatment may have a modulatory influence on myocardial cell hypertrophy in the context of HCM.

3.3 NLRP3 Inhibition Rescues Radiation-induced Cell Cytotoxicity

Considering the role of NLRP3 and the cGAS-STING pathway in the modulation of pyroptotic cell death within the context of cardiovascular disease [35], we proceeded to examine the impact of NLRP3 inhibition and cGAS overexpression on cell viability. HL-1 cardiomyocyte cells were divided into six experimental groups: a control group, a radiation group, a NLRP3 inhibitor (MCC950) + radiation group, a cGAS overexpression group, and a cGAS overexpression + MCC950 + radiation group. Initially, the effectiveness of radiation on HL-1 cells was assessed using SEM. As shown in Fig. 3B, X-ray irradiated HL-1 cells exhibited signs of plasma membrane rupture (indicated by red arrows) and a flattened cytoplasm, which are characteristic features of pyroptotic cells, in con-



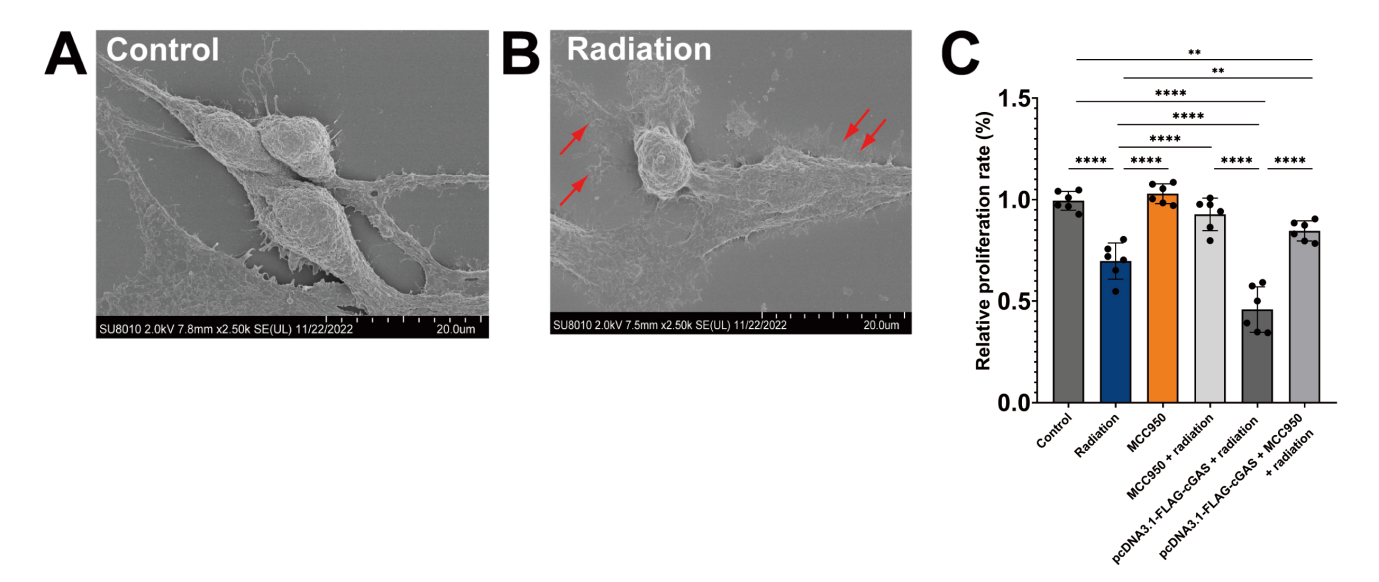


Fig. 3. NLR family pyrin domain containing 3 (NLRP3) inhibition rescues radiation-induced cell cytotoxicity. (A,B) Representative scanning electron microscopy (SEM) images of control HL-1 cells (A) and X-ray irradiated HL-1 cells (B). Red arrows indicate ruptured plasma membrane. The scale bar = 20 μ m. (C) Quantitative analysis of cell viability in HL-1 cells under different conditions. Cell viability was assessed by Cell Counting Kit-8 (CCK8) assay. Mean \pm SD, **p < 0.01, and ****p < 0.0001, compared to untreated HL-1 cells.

trast to the control cells depicted in Fig. 3A. This observation confirms that the cells experienced pyroptosis as a result of radiation exposure.

The results obtained from the CCK-8 assay confirmed that radiation significantly reduced cell viability in comparison to control groups, thereby illustrating the cytotoxic effects of radiation on HL-1 cells (p < 0.0001, Fig. 3C). The NLRP3 inhibitor (MCC950) did not exhibit any significant impact on cell viability when assessed alone against control cells. However, in HL-1 cells subjected to radiation, the administration of MCC950 markedly enhanced cell proliferation relative to the radiation only group (p < 0.0001), indicating a protective role of the NLRP3 inhibitor against radiation-induced cytotoxicity. Conversely, the overexpression of cGAS in cells exposed to radiation resulted in a further decline in cell viability compared to the radiation group, suggesting a harmful effect associated with cGAS overexpression. Notably, this detrimental effect was mitigated by the inhibition of NLRP3, as evidenced in the pcDNA3.1-FLAG-cGAS+MCC950+radiation group (Fig. 3C). These findings highlight the potential protective benefits of NLRP3 inhibition on cell viability following radiation exposure, while also emphasizing the adverse consequences of cGAS overexpression.

3.4 Radiation Induces Loss of Mitochondrial Membrane Potential and mtDNA Leak into Cytoplasm through cGAS/STING/NLRP3

Mitochondrial homeostasis plays a vital role in the regulation of pyroptosis. An overproduction of mitochondrial ROS can lead to the formation of macropore in the outer mitochondrial membrane of mitochondria and subsequent damage to mitochondrial DNA. This damage facilitates the release of mtDNA into the cytoplasm, which activates the cGAS-STING pathway, thereby promoting pyroptosis [21]. Therefore, our study sought to examine the impacts of radiation exposure, NLRP3 inhibition, and cGAS overexpression on mitochondrial membrane potential and morphology.

Staining with the JC-1 probe demonstrated that exposure to radiation resulted in a substantial reduction of mitochondrial membrane potential in HL-1 cells, as indicated by a significant decrease in the red/green fluorescence ratio (p < 0.0001) when compared to control cells (Fig. 4A). The JC-1 aggregates emitted red fluorescence, while the presence of green fluorescence signified the existence of JC-1 monomers. In contrast, the group treated with the NLRP3 inhibitor (MCC950) in conjunction with radiation exhibited a notable preservation of mitochondrial membrane potential relative to the radiation-only group (p < 0.001), implying a potential protective role of NLRP3 inhibition against radiation-induced mitochondrial impairment. Conversely, the overexpression of cGAS was found to further intensify the loss of mitochondrial membrane potential in cells subjected to X-ray irradiation compared to those exposed to radiation alone. Notably, NLRP3 inhibition significantly mitigated the detrimental effects of cGAS overexpression in X-ray irradiated cells (p < 0.0001). It is important to note that treatment of HL-1 cells with MCC950 alone did not influence mitochondrial membrane potential.

The labeling of biologically active mitochondria (indicated in red) and mtDNA (indicated in green) provided ev-



idence that radiation exposure significantly enhanced both the quantity of mitochondria and the release of mtDNA into the cytoplasm (Fig. 4B,D), as illustrated in Fig. 4B,C (p < 0.0001). Notably, the inhibition of NLRP3 using MCC950 in X-ray irradiated HL-1 cells resulted in a significant reduction in mitochondria quantity compared to the radiation-only group (p < 0.05, Fig. 4B,D,E,F). Furthermore, the overexpression of cGAS further intensified the increase in mitochondrial numbers relative to the radiation only group (Fig. 4B,D,G), while the application of MCC950 significantly alleviated this effect (p < 0.05, Fig. 4B,G,H). Collectively, these results suggest that radiation-induced oxidative stress disrupts mitochondrial membrane potential, facilitating the leakage of mtDNA, a process that is mediated by the cGAS/STING/NLRP3 signaling pathway.

3.5 Radiation Induces Pyroptosis through Activation of the cGAS/STING/NLRP3 Signalling Axis

The cGAS-STING signaling pathway plays a crucial role in the regulation of pyroptosis via NLRP3 inflammasomes [36]. In summary, the detection of cytosolic DNA by cGAS leads to the production of cGAMP, which initiates a cascade reaction within the cGAS-STING pathway, a process that is mediated by the NLRP3 inflammasome. The activation of NLRP3 subsequently recruits and activates caspase-1, which in turn activates the pro-inflammatory cytokines IL-1 β and IL-18, as well as GSDMD, a protein that forms membrane pores upon cleavage, ultimately resulting in pyroptotic cell death. The N-terminal fragment of GSDMD, referred to as GSDMD-N, is specifically responsible for the formation of these membrane pores, thereby compromising cellular integrity [5,37-39]. Additionally, we demonstrated that the overexpression of cGAS significantly elevated the levels of NLRP3 in normal HL-1 cells, thereby confirming the signaling cascades associated with the cGAS/STING/NLRP3 signaling axis (Supplementary Fig. 4A,B).

In light of the involvement of these proteins in cGAS/STING/NLRP3-mediated pyroptosis, an analysis of their levels was conducted in HL-1 cells through western blotting techniques. The findings from the western blot analysis revealed that the irradiation of HL-1 cells resulted in a marked upregulation of cGAS, STING, NLRP3, caspase-1, cleaved caspase-1, GSDMD, and GSDMD-N when compared to the control HL-1 cells (Fig. 5A–J).

Inhibition of NLRP3 in irradiated HL-1 cells led to a marked decrease in the levels of cleaved caspase-1 (p < 0.01, Fig. 5G) and GSDMD-N (p < 0.0001, Fig. 5J). Furthermore, the protein expression of NLRP3 was reduced in cells treated with MCC950, thereby confirming the efficacy of NLRP3 inhibition (p < 0.0001, Fig. 5D). Conversely, overexpression of cGAS in X-ray irradiated cells resulted in an exacerbation of all pyroptotic protein levels compared to radiation treatment alone, with significant increases observed in STING (p < 0.01), NLRP3 (p < 0.001),

caspase-1 (p < 0.001), cleaved caspase-1 (p < 0.01), GS-DMD (p < 0.01), and GSDMD-N (p < 0.001, Fig. 5A–J). Notably, the inhibition of NLRP3 reversed this trend, as indicated by the reduced levels of caspase-1, cleaved caspase-1, GSDMD, and GSDMD-N in the cGAS overexpression + radiation + MCC950 group compared to the cGAS overexpression and X-ray irradiation group (p < 0.0001, Fig. 5F–J). The levels of cGAS and STING remained constant across these two groups, reinforcing the hypothesis that NLRP3 functions downstream of the cGAS-STING signaling pathway (Fig. 5A–C). Collectively, these findings suggest that radiation-induced pyroptosis is mediated through the cGAS/STING/NLRP3 axis, and that NLRP3 inhibition can mitigate pyroptosis activated by the cGAS-STING pathway.

In alignment with these findings, the experiment involving HCM mice demonstrated comparable outcomes, as the group subjected to HCM and radiation exhibited significantly elevated protein levels of cGAS, STING, NLRP3, caspase-1, cleaved caspase-1, GSDMD, and GSDMD-N in comparison to the HCM-only group (Fig. 6A–J). This observation indicates the activation of the cGAS-STING signaling pathway in response to cellular stress induced by radiation. Conversely, it was unexpectedly noted that in the HCM mouse model, the performance of TAC surgery led to a reduction in the levels of pyroptotic proteins when compared to the sham-operated group (Fig. 6A–J).

3.6 NLRP3 Inhibition Attenuates the Production of IL-18 and IL-1 β

The concentration of cGAMP, the second messenger that binds to STING, was assessed using ELISA assays. In alignment with the observed trends in other pyroptotic proteins previously discussed, a notable increase in cGAMP levels was detected in mice subjected to HCM and radiation when compared to those with HCM alone (p < 0.05, Fig. 6K). In HL-1 cells, exposure to radiation resulted in elevated cGAMP levels relative to the control cells; however, this increase did not reach statistical significance. Additionally, NLRP3 did not appear to influence cGAMP levels in cells exposed to X-ray irradiation. While overexpression of cGAS seemed to elevate cGAMP levels, this increase was not statistically significant when compared to the group exposed solely to radiation (Fig. 6L).

As previously mentioned, IL-18 and IL-1 β serve as critical downstream mediators in the process of pyroptosis. As shown in Fig. 6M,N, the exposure to radiation resulted in a significant elevation of both IL-18 and IL-1 β levels in HL-1 cells (p < 0.001 and p < 0.01, respectively), thereby indicating the activation of the NLRP3 inflammasome in response to radiation-induced cellular stress. Conversely, the application of MCC950, an inhibitor of NLRP3, resulted in a marked reduction in the expression of IL-1 β and IL-18 in the presence of radiation. Furthermore, the overexpression of cGAS led to an increase in IL-1 β and IL-18



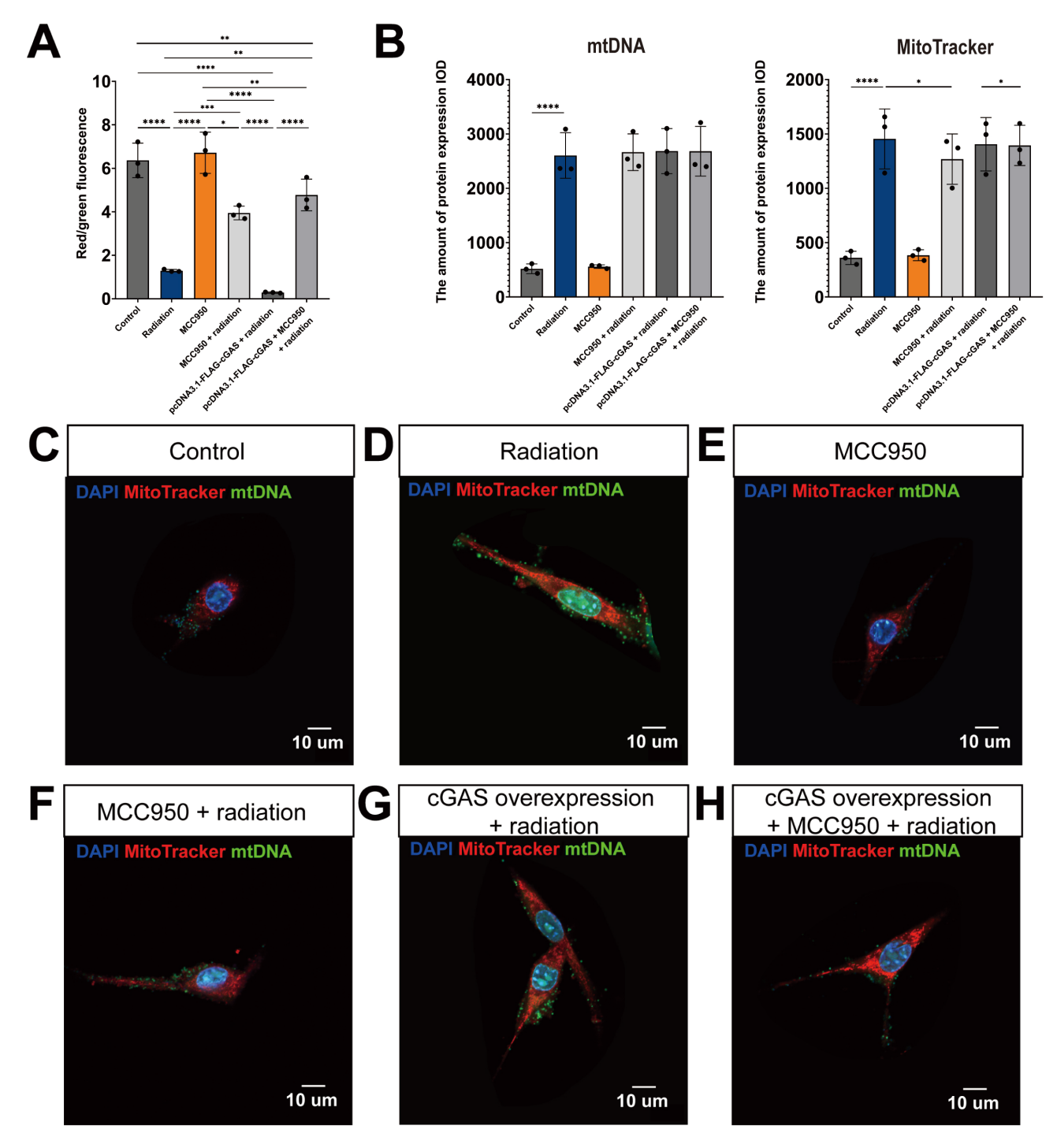


Fig. 4. Radiation-induced loss of mitochondrial membrane potential and mitochondrial DNA (mtDNA) leakage into the cytoplasm through activation of cyclic guanosine monophosphate-adenosine monophosphate (cGAMP) synthase (cGAS)/STING/NLRP3. (A) Quantitative analysis of mitochondrial membrane potential using JC-1 probe red/green fluorescence ratios in HL-1 cells. (B) The expression levels of mtDNA and MitoTracker under different conditions. Mean \pm SD, *p < 0.05, **p < 0.01, ***p < 0.001, and *****p < 0.0001, compared to untreated control HL-1 cells. (C–H) Representative images showing mitochondrial DNA (green) and mitochondria (red) in HL-1 cells under different conditions. The scale bar = 10 μ m. Nuclei were, DAPI (blue).

levels; however, this increase was mitigated by the inhibition of NLRP3, as evidenced in group subjected to cGAS overexpression, MCC950 treatment, and radiation exposure (Fig. 6M,N). Collectively, these findings underscore

the protective role of NLRP3 inhibition in mitigating pyroptosis through the downregulation of pro-inflammatory cytokine production.



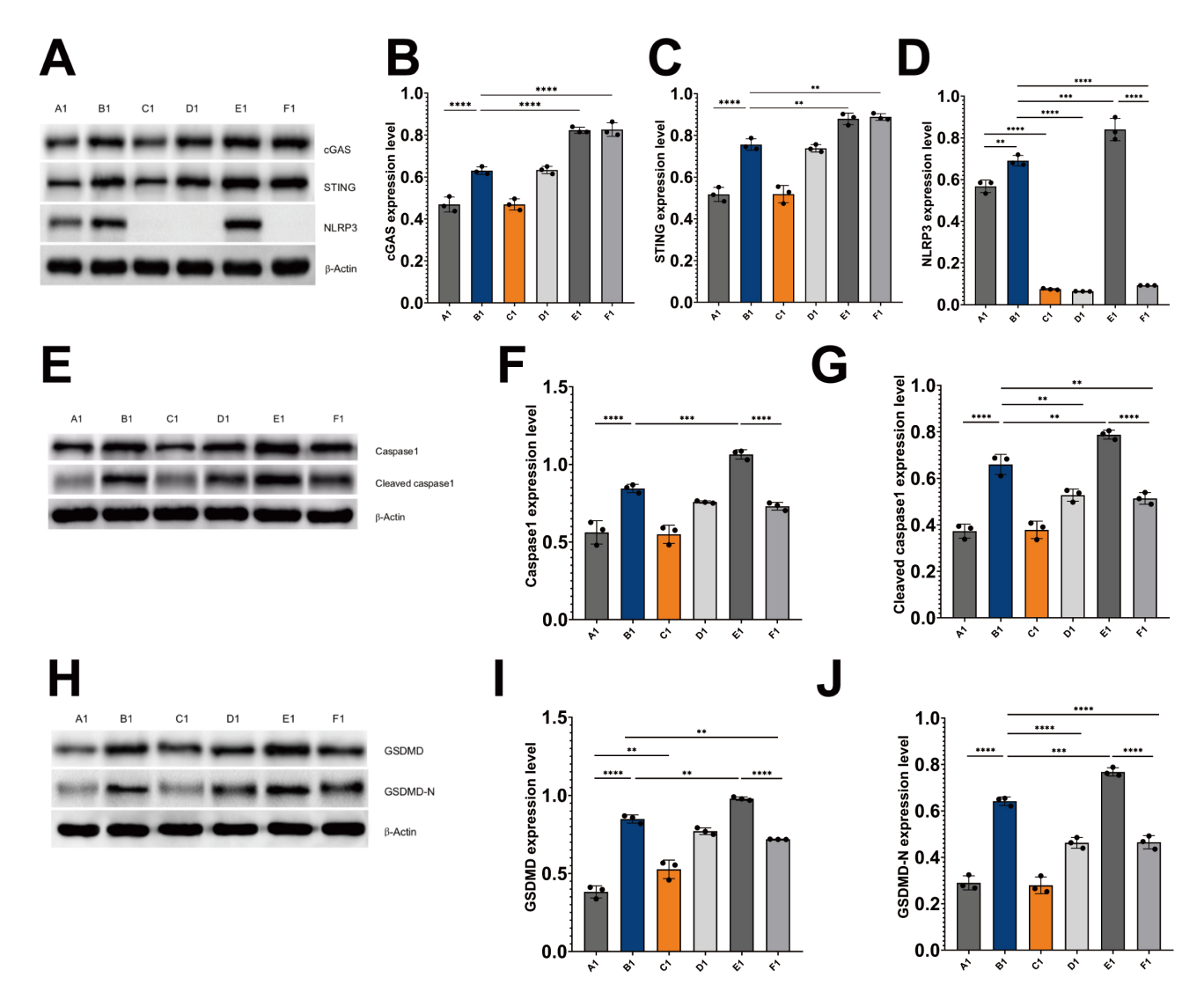


Fig. 5. Radiation induces pyroptosis through activation of cGAS/STING/NLRP3 axis in HL-1 cells. Immunoblots and histograms show the protein levels of cGAS, STING, NLRP3 (A–D), caspase-1, cleaved caspase-1 (E–G), GSDMD, and GSDMD-N (H–J) in different HL-1 cell treatment groups. A1: control HL-1 cells; B1: Irradiated HL-1 cells; C1: MCC950-treated HL-1 cells; D1: MCC950 + irradiated HL-1 cells; E1: cGAS overexpression + irradiated HL-1 cells; and F1: cGAS overexpression + MCC950 + irradiated HL-1 cells. Mean \pm SD, **p < 0.01, ***p < 0.001, and ****p < 0.0001.

4. Discussion

SBRT is a well-established treatment modality for cancer treatment [5]; however, its potential application in the management of non-malignant conditions, such as HCM, has recently gained attention [2,7]. The objective of this study was to explore the molecular mechanisms underlying cGAS/STING/NLRP3-mediated pyroptosis in the context of radiotherapy for HCM, utilizing both *in vivo* mouse models and *in vitro* cardiomyocyte experiments to provide foundational evidence for the radiobiological effects of SBRT. Our results indicated that radiation therapy enhanced cardiac function and reduced myocardial cell hypertrophy in a mouse model of HCM. Furthermore, we demonstrated that radiation-induced oxidative stress resulted in the leakage of mtDNA into the cytoplasm, which

subsequently activated the cGAS-STING signaling pathway. This activation ultimately led to pyroptosis of cardiomyocytes through the involvement of NLRP3 inflammasomes (Fig. 7).

cGAS functions as a cytoplasmic sensor for DNA, identifying cytosolic self-DNA, which includes damage-associated molecular patterns (DAMPs) such as mtDNA released from compromised mitochondria [37,38]. Upon interaction with DNA, cGAS binds to STING to form a complex, which also involves the synthesis of cGAMP. This interaction initiates the activation of the kinases TBK1 and IKK, leading to the subsequent activation of the transcription factors IRF3 and NF- κ B, respectively [40,41]. In alignment with previous studies [42,43], our findings indicate that exposure to radiation resulted in elevated levels of



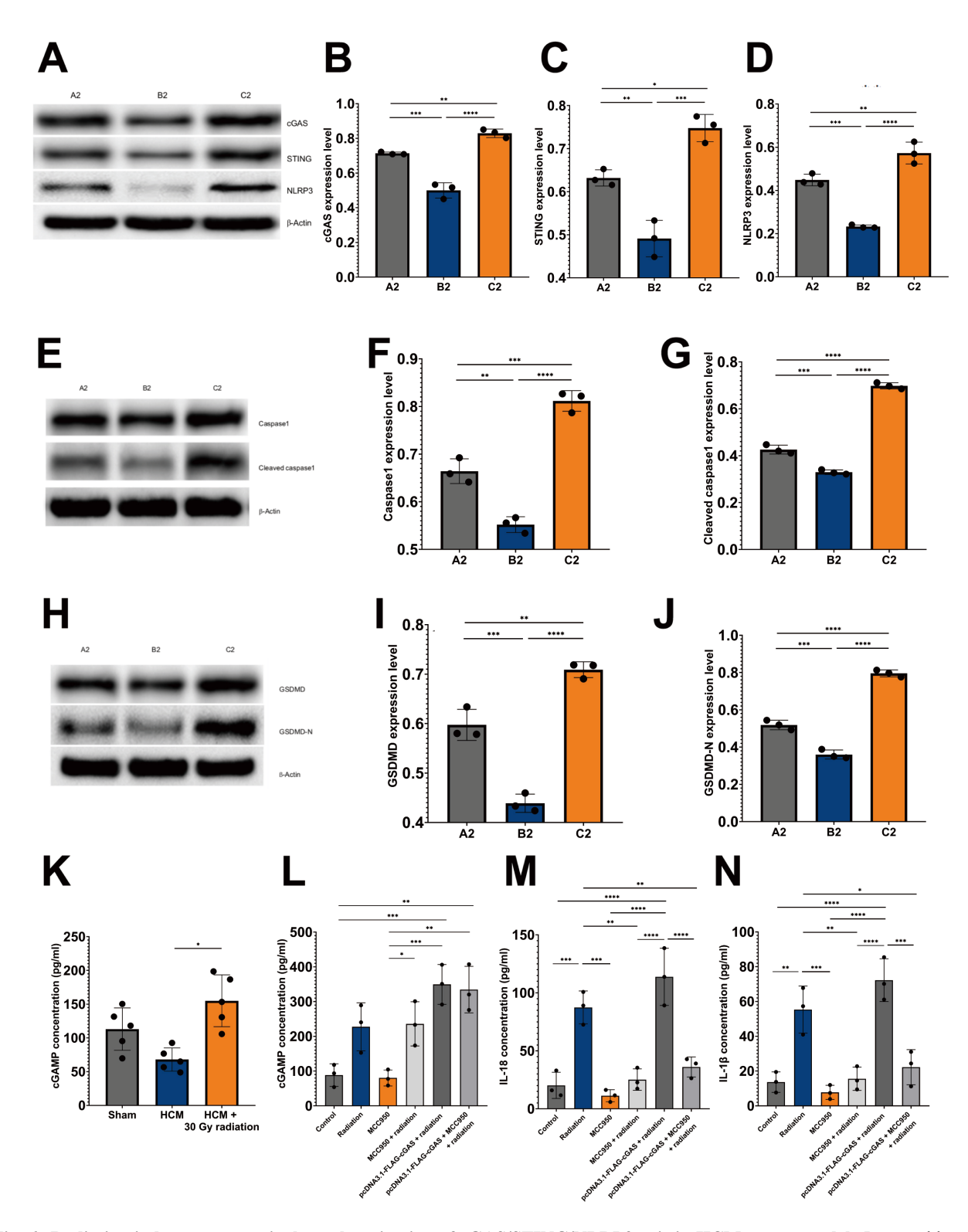


Fig. 6. Radiation induces pyroptosis through activation of cGAS/STING/NLRP3 axis in HCM mouse model. Immunoblots and histograms show the protein levels of cGAS, STING, NLRP3 (A–D), caspase-1, cleaved caspase-1 (E–G), GSDMD, and GSDMD-N (H–J) in three mouse experimental groups, n = 5 per group. A2: sham-operated mice; B2: pressure overload-induced HCM mice; C2: HCM + radiation mice. (K,L) Quantitative analysis of cGAMP levels in three experimental mouse groups (K), and HL-1 cells under different conditions (L). (M,N) Quantitative analysis of IL-18 (M) and IL-1 β (N) levels in HL-1 cells under different conditions. Mean \pm SD, *p < 0.05, **p < 0.01, ****p < 0.001, and *****p < 0.0001.

cGAS and STING, as well as an increase in other proteins associated with pyroptosis, including NLRP3, caspase-1, GSDMD, IL-18 and IL-1 β , in both HL-1 cells and an *in vivo* mouse model of HCM. These results support the involvement of the cGAS-STING-NLRP3 pathway in radiation-induced pyroptosis (Fig. 7).

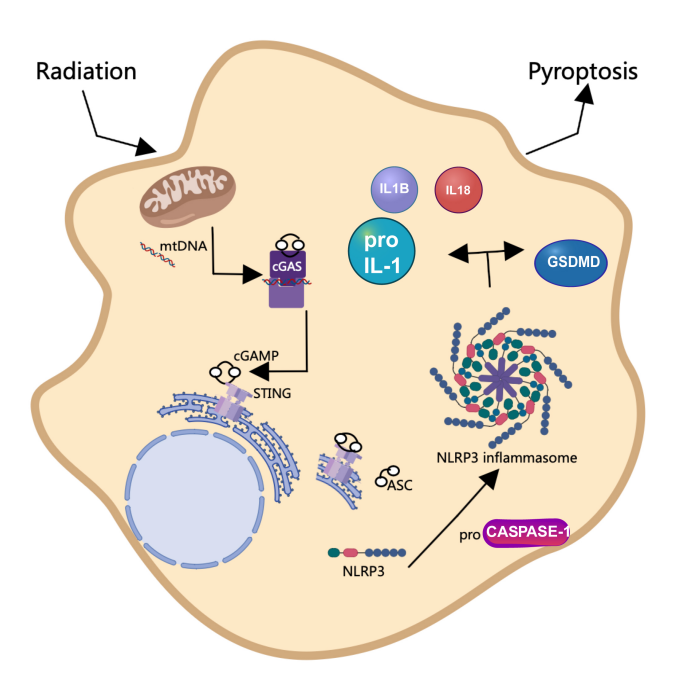


Fig. 7. Schematic diagram illustrating the effect of radiation on the initiation of pyroptosis via activation of the cGAS/STING/NLRP3 axis. Radiation exposure initiates oxidative stress, leading to the release of mitochondrial DNA (mtDNA) into the cytoplasm. This in turn activates the cGAS-STING pathway, triggering a cascade that involves the induction of pyroptosis-associated proteins. This intricate network underscores the radiation-induced mechanism leading to pyroptotic cell death. This figure was created using Microsoft PowerPoint (Version 16.52, Microsoft, Redmond, WA, USA) and Photoshop (CS6 version 13.0, Adobe, San Jose, CA, USA).

Furthermore, we provide mechanistic evidence indicating that the activation of the cGAS-STING pathway induces pyroptosis in cardiomyocyte and promotes the release of proinflammatory cytokines in a manner dependent on the NLRP3 inflammasome. Our results from *in vitro* experiments utilizing HL-1 cells demonstrated that exposure to radiation resulted in diminished cell viability, a notable reduction in mitochondrial membrane potential, and an increased presence of mtDNA in the cytoplasm. These adverse effects were alleviated by the inhibition of NLRP3 through the application of MCC950, a selective NLRP3 inhibitor, while exacerbation occurred with the overexpression of cGAS. This observation is consistent with prior research that established a relationship between cGAS-STING and NLRP3. In a model of cardiac injury induced by lipopolysaccha-

ride (LPS), Li et al. [44] reported that LPS-mediated stimulation of STING activated NLRP3, a process contingent upon the generation of ROS. Furthermore, the protective effects observed following STING silencing in LPS-treated cardiomyocytes were negated by NLRP3 overexpression [36]. Additionally, a separate investigation by Yan et al. [45] demonstrated that palmitic acid-induced lipotoxicity resulted in pyroptosis through the activation of the NLRP3 inflammasome via the cGAS-STING signaling cascade in myocardial cells, contributing to the pathogenesis of diabetic cardiomyopathy [45]. Interestingly, our in vivo investigation utilizing a mouse model of HCM induced by pressure overload indicates that radiation therapy may confer benefits in enhancing cardiac function and mitigating cardiomyocyte hypertrophy, as evidenced by echocardiographic assessments and WGA staining. These findings are consistent with prior research demonstrating favorable responses to SBRT treatment in clinical HCM patient populations [2,7]. Notably, while endpoints such as apoptosis, pyroptosis, and mitochondrial leakage are typically regarded as adverse consequences of radiation exposure, within the context of HCM, these phenomena may possess therapeutic potential. This is attributable to the direct and indirect cytotoxic effects of SBRT on aberrant cardiomyocytes, which can contribute to the reduction of left ventricular outflow tract obstruction and myocardial ischemia [15]. Although the observed "negative effects", including apoptosis and pyroptosis, may initially appear detrimental, they could serve a dual purpose by curtailing the excessive growth and proliferation of cardiomyocytes, thereby alleviating the hypertrophic condition. For example, the activation of pyroptosis via the cGAS/STING/NLRP3 signaling pathway may facilitate the clearance of damaged and hypertrophied cardiomyocytes, ultimately enhancing overall cardiac function.

It is important to recognize that the activation of the cGAS-STING pathway induced by radiation is complex and may result in various adverse therapeutic effects, such as resistance to radiotherapy due to immunosuppression, increased cell metastasis, and inflammatory conditions caused in non-diseased tissues [43]. Study on resistance to radio-immunotherapy indicates that the cGAS-STING pathway can be activated to facilitate cell death, which plays a role in combating tumor metastasis [23]. Nevertheless, as a critical regulatory axis of mitochondrial function in maintaining cellular homeostasis, the cGAS-STING pathway is vital for the activation of autophagy, which helps restore restores mitochondrial homeostasis [37,46,47]. Furthermore, while radiotherapy has been employed in the treatment of cardiac arrhythmias [48,49], there remains a paucity of information regarding its clinical effectiveness in the management of HCM. Therefore, it is crucial to clarify the molecular mechanisms through which radiotherapy mitigates HCM and to ensure that clinical applications are conducted safely and effectively. Furthermore, in the cur-



rent study, we have demonstrated that the mouse model of pressure overload-induced HCM, established through TAC surgery, exhibited lower levels of cGAS-STING compared to the sham-operated mice. This finding contrasts with a prior study that indicated TAC surgery activated cGAS-STING signaling to promote pyroptosis [35].

In summary, our study offers novel insights into the therapeutic potential of targeting the cGAS/STING/NLRP3 pathway in HCM. We demonstrate that SBRT can activate this pathway, leading to pyroptosis and a reduction in cardiac hypertrophy, thereby elucidating a novel mechanism by which radiation therapy may be beneficial in the context of cardiovascular diseases. This discovery not only enhances our understanding of the pathophysiological mechanisms underlying HCM but also provides a foundation for the development of therapies based on pyroptosis. However, our study is not without limitations. Primarily, it was conducted using animal models and cell lines, which may not fully represent the complexities of the human cardiovascular system. Future research utilizing human samples and primary cells is essential to validate the effects of radiation on cGAS/STING/NLRP3-mediated pyroptosis in HCM. Furthermore, the impact of inhibiting or overexpressing of cGAS/STING/NLRP3 on radiation-induced pyroptosis warrants investigation in vivo, alongside assessments of cardiac function and myocardial morphology following radiation treatment combined with modulation of cGAS/STING/NLRP3 signaling. Furthermore, it would also be advantageous to explore the levels of ASC, a key component of the NLRP3 inflammasome. Lastly, future studies should also examine how inflammation induced by the cGAS-STING pathway may contribute to the repair of HCM and the downstream signaling mechanisms involved in HCM treatment via SBRT.

5. Conclusion

In conclusion, this research offers significant contributions to the understanding of the cGAS/STING/NLRP3 pathway-mediated pyroptosis in the context of radiotherapy for HCM. Our findings indicate that radiation not only enhances cardiac function but also induces oxidative stress, leading to mtDNA leakage. This leakage activates the cGAS-STING pathway, subsequently promoting pyroptosis in cardiomyocytes. The results suggest that the cGAS-STING pathway may represent a viable therapeutic target for mitigating radiation-induced cardiomyocyte damage to cardiomyocytes in HCM and other cardiovascular conditions. Further investigation is warranted to comprehensively assess the impact of activating or inhibiting critical components of the cGAS-STING signaling pathway on the effectiveness of radiotherapy. A deeper understanding the role of the cGAS/STING/NLRP3 pathway's role in HCM could facilitate the development of targeted therapies that replicate the advantageous effects of radiation. For example, the design of small molecule inhibitors or activators of this pathway could selectively induce pyroptosis in hypertrophic cardiomyocytes, thereby alleviating the pathological hypertrophy without resorting to invasive interventions. Moreover, these findings may contribute to the identification of biomarkers for the early diagnosis and prognosis of HCM, thereby improving enhancing patient stratification and enabling personalized treatment approaches.

Availability of Data and Materials

The datasets generated during the current study are available from the corresponding author under reasonable requests.

Author Contributions

The study conception and design were performed by HYL and JL. Experiment, material preparation, data collection and analysis were performed by HYL, XW, XPL, HMS, and JL. The first draft of the manuscript was written by HYL. All authors contributed to editorial changes in the manuscript. All authors read and approved the final manuscript. All authors have participated sufficiently in the work and agreed to be accountable for all aspects of the work.

Ethics Approval and Consent to Participate

The present study was approved by the ethics committee of Huashan Hospital of Fudan University (No 2020 Huashan Hospital JS-590). The mice were humanely care for and routinely fed according to the criteria outlined in the Guide for the Care and Use of Laboratory Animals from the National Institutes of Health (NIH).

Acknowledgment

We thank all the peer reviewers for their opinions and suggestions.

Funding

This research received no external funding.

Conflict of Interest

The authors declare no conflict of interest.

Supplementary Material

Supplementary material associated with this article can be found, in the online version, at https://doi.org/10.31083/FBL26084.

References

- [1] Bai Y, Zheng J-P, Lu F, Zhang X-L, Sun C-P, Guo W-H, *et al.* Prevalence, incidence and mortality of hypertrophic cardiomy-opathy based on a population cohort of 21.9 million in China. Scientific Reports. 2022; 12: 18799. https://doi.org/10.1038/s41598-022-20042-9.
- [2] Li HY, Wu JJ, Zhou P, Shi HM, Li J, Wang X, *et al.* The basic research and clinical exploration on the stereotactic radiotherapy



- (cyber knife) in hypertrophic cardiomyopathy. Fudan University Journal of Medical Sciences. 2022; 49: 360–368, 383. https://doi.org/10.3969/j.issn.1672-8467.2022.03.007. (In Chinese)
- [3] Rossano JW, Lin KY. Hypertrophic Cardiomyopathy: A Problem at Any Age. Journal of the American College of Cardiology. 2022; 79: 1998–2000. https://doi.org/10.1016/j.jacc.2022.03.356.
- [4] Maron BJ, Desai MY, Nishimura RA, Spirito P, Rakowski H, Towbin JA, *et al.* Management of Hypertrophic Cardiomyopathy: JACC State-of-the-Art Review. Journal of the American College of Cardiology. 2022; 79: 390–414. https://doi.org/10.1016/j.jacc.2021.11.021.
- [5] Ma L, Wang L, Tseng C-L, Sahgal A. Emerging technologies in stereotactic body radiotherapy. Chinese Clinical Oncology. 2017; 6: S12. https://doi.org/10.21037/cco.2017.06.19.
- [6] Park JS, Choi Y. Stereotactic Cardiac Radiation to Control Ventricular Tachycardia and Fibrillation Storm in a Patient with Apical Hypertrophic Cardiomyopathy at Burnout Stage: Case Report. Journal of Korean Medical Science. 2020; 35: e200. https://doi.org/10.3346/jkms.2020.35.e200.
- [7] Whitaker J, Mak RH, Zei PC. Non-invasive ablation of arrhythmias with stereotactic ablative radiotherapy. Trends In Cardiovascular Medicine. 2022; 32: 287–296. https://doi.org/10.1016/ j.tcm.2021.04.008.
- [8] Lowe HC, Oesterle SN, Khachigian LM. Coronary in-stent restenosis: current status and future strategies. Journal of the American College of Cardiology. 2002; 39: 183–193.
- [9] Pokhrel D, Sood S, McClinton C, Saleh H, Badkul R, Jiang H, et al. Linac-based stereotactic radiosurgery (SRS) in the treatment of refractory trigeminal neuralgia: Detailed description of SRS procedure and reported clinical outcomes. Journal of Applied Clinical Medical Physics. 2017; 18: 136–143. https://doi.org/10.1002/acm2.12057.
- [10] Hamdi H, Ferrante P, Spatola G, Clawson W, McGonigal A, Daquin G, et al. Epileptic hypothalamic hamartomas impact of topography on clinical presentation and radiosurgical outcome. Epilepsy Research. 2021; 173: 106624. https://doi.org/10.1016/ j.eplepsyres.2021.106624.
- [11] Jacob J, Reyns N, Valéry CA, Feuvret L, Simon JM, Mazeron JJ, et al. Radiotherapy of non-tumoral refractory neurological pathologies. Cancer Radiotherapie: Journal de La Societe Francaise de Radiotherapie Oncologique. 2020; 24: 523–533. https://doi.org/10.1016/j.canrad.2020.06.012.
- [12] Timmerman RD, Kavanagh BD, Cho LC, Papiez L, Xing L. Stereotactic body radiation therapy in multiple organ sites. Journal of Clinical Oncology: Official Journal of the American Society of Clinical Oncology. 2007; 25: 947–952.
- [13] Wei C, Qian P, Tedrow U, Mak R, Zei PC. Non-invasive Stereotactic Radioablation: A New Option for the Treatment of Ventricular Arrhythmias. Arrhythmia & Electrophysiology Review. 2020; 8: 285–293. https://doi.org/10.15420/aer.2019.04.
- [14] Kim E-J, Davogustto G, Stevenson WG, John RM. Non-invasive Cardiac Radiation for Ablation of Ventricular Tachycardia: a New Therapeutic Paradigm in Electrophysiology. Arrhythmia & Electrophysiology Review. 2018; 7. https://doi.org/10.15420/ae r.7.1.EO1.
- [15] Li X, Zhu Z, Liu J, Gao Y, Xiao Y, Fang Z, et al. Septal radioablation therapy for patients with hypertrophic obstructive cardiomyopathy: first-in-human study. European Heart Journal Open. 2023; 3: oead052. https://doi.org/10.1093/ehjopen/oead052.
- [16] Zhang K, Xu T, Wang JL. Progress in the application of stereotactic radiotherapy in nontumor diseases. Electronic Journal of Medical Operations. 2024; 11: 56–60. (In Chinese)
- [17] Shoji M, Inaba K, Itami J, Hamada M, Okamoto H, Iwasa T, et al. Advantages and challenges for noninvasive atrial fibrillation

- ablation. Journal of Interventional Cardiac Electrophysiology: an International Journal of Arrhythmias and Pacing. 2021; 62: 319–327. https://doi.org/10.1007/s10840-020-00904-w.
- [18] Nickoloff JA, Sharma N, Allen CP, Taylor L, Allen SJ, Jaiswal AS, et al. Roles of homologous recombination in response to ionizing radiation-induced DNA damage. International Journal of Radiation Biology. 2023; 99: 903–914. https://doi.org/10.1080/09553002.2021.1956001.
- [19] Park MW, Cha HW, Kim J, Kim JH, Yang H, Yoon S, et al. NOX4 promotes ferroptosis of astrocytes by oxidative stressinduced lipid peroxidation via the impairment of mitochondrial metabolism in Alzheimer's diseases. Redox Biology. 2021; 41: 101947. https://doi.org/10.1016/j.redox.2021.101947.
- [20] Hopfner KP, Hornung V. Molecular mechanisms and cellular functions of cGAS-STING signalling. Nature Reviews Molecular Cell Biology. 2020; 2: 501–521. https://doi.org/10.1038/ s41580-020-0244-x.
- [21] Yu C-H, Davidson S, Harapas CR, Hilton JB, Mlodzianoski MJ, Laohamonthonkul P, et al. TDP-43 Triggers Mitochondrial DNA Release via mPTP to Activate cGAS/STING in ALS. Cell. 2020; 183. https://doi.org/10.1016/j.cell.2020.09.020.
- [22] McLaughlin M, Patin EC, Pedersen M, Wilkins A, Dillon MT, Melcher AA, et al. Inflammatory microenvironment remodelling by tumour cells after radiotherapy. Nature Reviews. Cancer. 2020; 20: 203–217. https://doi.org/10.1038/s41568-020-0246-1.
- [23] Yi L, Jiang X, Zhou Z, Xiong W, Xue F, Liu Y, et al. A Hybrid Nanoadjuvant Simultaneously Depresses PD-L1/TGFβ1 and Activates cGAS-STING Pathway to Overcome Radio-Immunotherapy Resistance. Advanced Materials (Deerfield Beach, Fla.). 2024; 36: e2304328. https://doi.org/10.1002/adma .202304328.
- [24] Gaidt MM, Ebert TS, Chauhan D, Ramshorn K, Pinci F, Zuber S, et al. The DNA Inflammasome in Human Myeloid Cells Is Initiated by a STING-Cell Death Program Upstream of NLRP3. Cell. 2017; 171: 1110-1124.e18. https://doi.org/10.1016/j.cell.2017. 09.039
- [25] Gröschel MI, Sayes F, Shin SJ, Frigui W, Pawlik A, Orgeur M, et al. Recombinant BCG Expressing ESX-1 of Mycobacterium marinum Combines Low Virulence with Cytosolic Immune Signaling and Improved TB Protection. Cell Reports. 2017; 18: 2752-2765. https://doi.org/10.1016/j.celrep.2017.02.057
- [26] Ding R, Li H, Liu Y, Ou W, Zhang X, Chai H, et al. Activating cGAS-STING axis contributes to neuroinflammation in CVST mouse model and induces inflammasome activation and microglia pyroptosis. Journal of Neuroinflammation. 2022; 19: 137. https://doi.org/10.1186/s12974-022-02511-0.
- [27] Gao C, Xu Y-J, Qi L, Bao Y-F, Zhang L, Zheng L. CircRNA VIM silence synergizes with sevoflurane to inhibit immune escape and multiple oncogenic activities of esophageal cancer by simultaneously regulating miR-124/PD-L1 axis. Cell Biology and Toxicology. 2022; 38: 825–845. https://doi.org/10.1007/s1056-021-09613-0.
- [28] Ketelut-Carneiro N, Fitzgerald KA. Apoptosis, Pyroptosis, and Necroptosis-Oh My! The Many Ways a Cell Can Die. Journal of Molecular Biology. 2022; 434: 167378. https://doi.org/10.1016/ j.jmb.2021.167378.
- [29] Toldo S, Abbate A. The role of the NLRP3 inflammasome and pyroptosis in cardiovascular diseases. Nature Reviews. Cardiology. 2024; 21: 219–237. https://doi.org/10.1038/ s41569-023-00946-3.
- [30] deAlmeida AC, van Oort RJ, Wehrens XHT. Transverse aortic constriction in mice. Journal of Visualized Experiments: JoVE. 2010. https://doi.org/10.3791/1729.
- [31] Sørensen LL, Bedja D, Sysa-Shah P, Liu H, Maxwell A, Yi X, et al. Echocardiographic Characterization of a Murine Model of



- Hypertrophic Obstructive Cardiomyopathy Induced by Cardiacspecific Overexpression of Epidermal Growth Factor Receptor 2. Comparative Medicine. 2016; 66: 268–277.
- [32] Herr DR, Yam TYA, Tan WSD, Koh SS, Wong WSF, Ong W-Y, et al. Ultrastructural Characteristics of DHA-Induced Pyroptosis. Neuromolecular Medicine. 2020; 22: 293–303. https://doi.org/10.1007/s12017-019-08586-y.
- [33] Stern AD, Rahman AH, Birtwistle MR. Cell size assays for mass cytometry. Cytometry. Part A: the Journal of the International Society For Analytical Cytology. 2017; 91: 14–24. https://doi. org/10.1002/cyto.a.23000.
- [34] Xiong X-Y, Tang Y, Yang Q-W. Metabolic changes favor the activity and heterogeneity of reactive astrocytes. Trends In Endocrinology and Metabolism: TEM. 2022; 33: 390–400. https://doi.org/10.1016/j.tem.2022.03.001.
- [35] Yue R, Zheng Z, Luo Y, Wang X, Lv M, Qin D, et al. NLRP3-mediated pyroptosis aggravates pressure overload-induced cardiac hypertrophy, fibrosis, and dysfunction in mice: cardio-protective role of irisin. Cell Death Discovery. 2021; 7: 50. https://doi.org/10.1038/s41420-021-00434-y.
- [36] Zhang W, Li G, Luo R, Lei J, Song Y, Wang B, et al. Cytosolic escape of mitochondrial DNA triggers cGAS-STING-NLRP3 axis-dependent nucleus pulposus cell pyroptosis. Experimental & Molecular Medicine. 2022; 54: 129–142. https://doi.org/10.1038/s12276-022-00729-9.
- [37] Chen C, Xu P. Cellular functions of cGAS-STING signaling. Trends In Cell Biology. 2023; 33: 630–648. https://doi.org/10.1016/j.tcb.2022.11.001.
- [38] Zhang X, Bai X-C, Chen ZJ. Structures and Mechanisms in the cGAS-STING Innate Immunity Pathway. Immunity. 2020; 53: 43–53. https://doi.org/10.1016/j.immuni.2020.05.013.
- [39] Blevins HM, Xu Y, Biby S, Zhang S. The NLRP3 Inflammasome Pathway: A Review of Mechanisms and Inhibitors for the Treatment of Inflammatory Diseases. Frontiers In Aging Neuroscience. 2022; 14: 879021. https://doi.org/10.3389/fnagi.2022. 879021.
- [40] Zhang M, Zou Y, Zhou X, Zhou J. Inhibitory targeting cGAS-STING-TBK1 axis: Emerging strategies for autoimmune diseases therapy. Frontiers In Immunology. 2022; 13: 954129. https://doi.org/10.3389/fimmu.2022.954129.
- [41] Oduro PK, Zheng X, Wei J, Yang Y, Wang Y, Zhang H, et al.

- The cGAS-STING signaling in cardiovascular and metabolic diseases: Future novel target option for pharmacotherapy. Acta Pharmaceutica Sinica. B. 2022; 12: 50–75. https://doi.org/10.1016/j.apsb.2021.05.011.
- [42] Han D, Zhang J, Bao Y, Liu L, Wang P, Qian D. Anlotinib enhances the antitumor immunity of radiotherapy by activating cGAS/STING in non-small cell lung cancer. Cell Death Discovery. 2022; 8: 468. https://doi.org/10.1038/ s41420-022-01256-2.
- [43] Storozynsky Q, Hitt MM. The Impact of Radiation-Induced DNA Damage on cGAS-STING-Mediated Immune Responses to Cancer. International Journal of Molecular Sciences. 2020; 21. https://doi.org/10.3390/ijms21228877.
- [44] Li N, Zhou H, Wu H, Wu Q, Duan M, Deng W, et al. STING-IRF3 contributes to lipopolysaccharide-induced cardiac dysfunction, inflammation, apoptosis and pyroptosis by activating NLRP3. Redox Biology. 2019; 24: 101215. https://doi.org/10.1016/j.redox.2019.101215.
- [45] Yan M, Li Y, Luo Q, Zeng W, Shao X, Li L, et al. Mitochondrial damage and activation of the cytosolic DNA sensor cGAS-STING pathway lead to cardiac pyroptosis and hypertrophy in diabetic cardiomyopathy mice. Cell Death Discovery. 2022; 8: 258. https://doi.org/10.1038/s41420-022-01046-w.
- [46] Kim Y, Li C, Gu C, Fang Y, Tycksen E, Puri A, et al. MANF stimulates autophagy and restores mitochondrial homeostasis to treat autosomal dominant tubulointerstitial kidney disease in mice. Nature Communications. 2023; 14: 6493. https://doi.org/ 10.1038/s41467-023-42154-0.
- [47] Jia M, Qin D, Zhao C, Chai L, Yu Z, Wang W, et al. Redox home-ostasis maintained by GPX4 facilitates STING activation. Nature Immunology. 2020; 21: 727–735. https://doi.org/10.1038/s41590-020-0699-0.
- [48] Cuculich PS, Schill MR, Kashani R, Mutic S, Lang A, Cooper D, et al. Noninvasive Cardiac Radiation for Ablation of Ventricular Tachycardia. The New England Journal of Medicine. 2017; 377: 2325–2336. https://doi.org/10.1056/NEJMoa1613773.
- [49] Zeng L-J, Huang L-H, Tan H, Zhang H-C, Mei J, Shi H-F, *et al.* Stereotactic body radiation therapy for refractory ventricular tachycardia secondary to cardiac lipoma: A case report. Pacing and Clinical Electrophysiology: PACE. 2019; 42: 1276–1279. https://doi.org/10.1111/pace.13731.

